arXiv:1110.5604v1 [physics.optics] 25 Oct 2011

Flat-face approximations of invisibility cloaks with planar metamaterial layers

Oliver Paul[1], Yaroslav Urzhumov[2], Christoffer Elsen[1], David Smith[2], and Marco Rahm[1,3]

[1]Department of Physics and Research Center OPTIMAS, University of Kaiserslautern, 67663 Kaiserslautern, Germany

[2]Center for Metamaterials and Integrated Plasmonics, Pratt School of Engineering, Duke University, Durham, NC 27708, USA

[3]Fraunhofer Institute for Physical Measurement Techniques IPM, 79110 Freiburg, Germany

E-mail: paul@physik.uni-kl.de

Abstract. Transformation optics (TO) is a powerful tool for the design of artificial materials with unprecedented optical properties. General TO media are demanding, requiring spatially varying constitutive tensors with both anisotropic electric and magnetic response. Though metamaterials have been proposed as a path to achieving such complex media, the required properties corresponding to the most general transformations remain elusive even in metamaterials leveraging state-of-the-art fabrication methods. Fortunately, in many situations the most significant benefits of a TO medium can be obtained even if approximations to the ideal structures are employed. Here, we propose the approximation of TO structures of arbitrary shape by faceting, in which curved surfaces are approximated by flat metamaterial layers that can be implemented by standard fabrication and stacking techniques. We illustrate the approximation approach for the specific example of a cylindrical "invisibility cloak". First, we introduce a numerical method for the design of cloaks with arbitrary boundary shapes, and apply it to faceted shapes. Subsequently, we reduce the complexity of the metamaterials needed to implement the perfect faceted cloak by introducing several approximations, whose validity is quantified by an investigation of the scattering cross section.

PACS numbers: 42.15.Dp, 42.15.Eq, 42.25.Bs

1. Introduction

In recent years, the concept of transformation optics (TO) has emerged as a powerful tool for the control and manipulation of light [1, 2]. Based on the form-invariance of Maxwell's equations under coordinate transformation, TO is a tool in which the design of electromagnetic materials can be performed conceptually by applying a coordinate transformation to modify the trajectories of waves. By applying the desired coordinate

transformation to Maxwell's equations, the prescription for a medium can be obtained for which light propagates as if it was propagating in a different coordinate system [3]. One of the more compelling concepts to emerge from the TO approach has been that of cloaking [4–7]. The TO cloak arises from a transformation in which a region of space is effectively shrunk to a point or singularity, where its scattering becomes significantly reduced. The effect of the transformation is that waves appear to be guided around the "cloaked" region of space, rendering both the bounding TO medium and the cloaked region invisible to an external observer. Since the first experimental realization demonstration of a metamaterial cloak [4], cloaking devices have been proposed for nearly any imaginable geometry, including spheres [8, 9], circular cylinders [4, 10, 11], cylinders of square cross-section [12, 13] and also asymmetric and irregular shapes [14–18].

Though the coordinate transformations that lead to TO media are often arrived at intuitively and can be simply described, the physical implementation of TO media are typically challenging. In fact, while the mathematics of TO has been known for more than a century, TO has only been deemed relevant in the context of the ongoing development of artificially structured metamaterials over the past decade [19]. Metamaterials are artificial media, often consisting of arrays of metallic inclusions whose size and spacing are significantly smaller than the free space wavelength. Under these conditions, metamaterials can be described using effective constitutive parameter tensors. TO media are specified by spatially varying distributions of the permittivity and permeability tensors that derive from coordinate transformations. To implement these distributions using metamaterials, the continuously varying constitutive parameters are discretized throughout space and an appropriate metamaterial design is chosen that achieves the desired constitutive tensor elements at each discrete spatial point. Finding the appropriate metamaterial element at each point, however, is a challenging task since nearly arbitrary control is required over each of the electric and magnetic responses along six principal axes. For a given polarization, the number of controlled responses reduces to three for a complete TO solution, which still represents a significant challenge.

A reduction in the complexity of a TO structure can be obtained if some of the performance is sacrificed. For example, the trajectory of a wave can be managed solely by a spatially varying, anisotropic index of refraction [4, 20]. By giving up the ability to control the wave impedance of a medium, which implies a loss of control over reflection, one gains much more freedom in the transformation and hence the material properties. For example, the need for magnetic (or electric) response can be eliminated if only the refractive index is to be varied. This form of approximation has been termed the "eikonal" approximation [21]. Eikonal cloaks and other TO structures have been introduced that have more potential routes to implementation, including the use of photonic crystals [20].

The experimental implementation is further complicated if the cloak possesses curved contours. A conformal cloak designed to conceal a region of arbitrary shape generally leads to a curvilinear alignment of the principal axes of the permittivity and

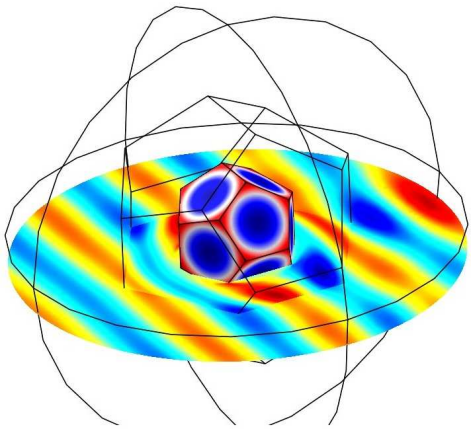

Figure 1. (Color online) Full-wave simulation: faceted dodecahedral approximation to the full-parameter spherical cloak, obtained by truncating the sphere circumscribing a regular dodecahedron. No correction to the material property distribution was made.

permeability tensors, resulting in a gradual rotation of the local metamaterial elements throughout space. The metamaterial architecture for such designs can be surprisingly complex in all but the most symmetric designs. Even for highly symmetric designs, such as that of a spherical metamaterial, the fabrication can pose a significant hurdle. Since most fabrication techniques are suited for the production of planar samples, it is of considerable advantage to seek approximation methods that will leverage standard and commercial lithographic patterning [19]. For TO devices operating at microwave [4] and THz [22] frequencies, cylindrical device shapes can be obtained by curling planar sheets of metamaterials. However, as the operational frequency increases towards the optical range and the metamaterial layer thickness decreases to micro- and nanometer scale, this approach becomes impractical. As for TO devices with fully three-dimensional shapes, such as spherical cloaks, curving planar-layer metamaterials is not a viable approach even for microwave frequencies. While substantial progress is being made towards volumetric three-dimensional metamaterial fabrication methods [19], the contemporary techniques remain prohibitively difficult to use for structures that cannot be conceived as "sandwiched" flat layers of meta-elements. For three-dimensional TO devices such as the one shown in figure 1 faceted approximations are therefore essential.

The route to more feasible TO media considered here is the substitution of an arbitrary TO structure, which may have curved surfaces, with a polygonal (in two dimensions) or polyhedral (in 3D) approximation. To apply the method, we first start with an exact transformation of a two-dimensional TO device of arbitrary shape. Next, the resulting structure—which may have curved surfaces—is approximated by polygons with an increasing number of vertices. Clearly, as the number of vertices increases, the error in the approximation should decrease, eventually becoming negligible. The tradeoff is to find the polygon approximation with the minimum number of vertices that will provide acceptable performance; such a structure will be achievable by assembling a

limited number of planar sections together. The metamaterial element is identical in each planar layer, both in terms of shape as well as orientation.

As a secondary refinement to the faceted approximation, the specific orientation of the metamaterial elements within each planar layer can be properly taken into account by using a transformation that maps exactly to the faceted shape. For such media, metamaterial elements whose principal axes are coincident with the planar layer can be readily implemented, whereas other metamaterial elements whose principal axes are not coincident with the planar layer will necessarily complicate the fabrication steps or even preclude a proper fabrication of the TO device.

The metamaterial invisibility cloak provides a useful structure for investigating the performance of faceted approximations, because it can be well-characterized by a single figure-of-merit: the (total) scattering cross-section (SCS) [21, 23]. For this reason, we choose the cloaking transformation as the illustrative example, testing the performance of a variety of faceted approximations. In Section 2, we introduce two coordinate transformation approaches for the design of arbitrary-shape cloaks. The proposed methods are quite general and can be applied to irregular, convex and non-convex shapes, including to some extent shapes with sharp corners. We show that these methods can be used to design ideal cloaks with flat, polygonal surfaces. In Section 3, we introduce a polygonal approximation scheme for TO devices of arbitrary shapes, using the cylindrical cloak of invisibility as a test bed application. We evaluate and quantify the effect of the different approximation steps by calculating the total scattering cross section (SCS) of the approximate cloaks, and compare the results to the SCS of the exact TO cloak. We discuss in detail the dependence of the SCS on the geometric parameters and the parameters introduced by the approximations, including the size of the cloak, the number of layers, the number of sectors in the polygonal approximation, and the angle of incidence with respect to the polygon orientation.

2. Transformation optics of arbitrary-shape cloaks

We restrict our analysis to two-dimensional (in-plane) wave propagation through cylindrical cloaks, possibly with non-circular cross-section. Additionally, we assume that the incident wave is a monochromatic TE-polarized wave, that is, a wave whose electric field vector is parallel to the cylinder axis (z-axis) and the wave vector is normal to it. For a cloak whose inner and outer boundaries are circular, the exact TO solution is well-known [4, 5]. For the particular case of a linear, radial transformation of the form

$$r' = \frac{b(r-a)}{b-a}, \quad \phi' = \phi, \tag{1}$$

the relevant tensor components of the permittivity and permeability take the form:

$$\epsilon_z(r) = \left(\frac{b}{b-a}\right)^2 \frac{r-a}{r}, \quad \mu_r(r) = \frac{r-a}{r}, \quad \mu_\phi(r) = \frac{r}{r-a} \tag{2}$$

where a and b are the inner and the outer radius of the cloak, respectively.

As described in the introduction, in certain circumstances one may trade the perfectly non-reflecting properties of ideal TO structures for a reduced fabrication burden. In the eikonal approximation, only the refractive indexes given by $n_\phi = \sqrt{\epsilon_z \mu_r}$ and $n_r = \sqrt{\epsilon_z \mu_\phi}$ are relevant to the wave propagation inside the cloak [24]. An eikonal cloak can be derived from an exact cloak, such as the one given by (2), in an infinite number of ways. For example, one can fix $\mu_\phi \equiv 1$, in which case the cloak governed by a linear transformation is described by the following constitutive parameters [4, 5]:

$$\epsilon_z = \left(\frac{b}{b-a}\right)^2, \quad \mu_r(r) = \left(\frac{r-a}{r}\right)^2, \quad \mu_\phi = 1. \tag{3}$$

With the reduced parameter set, the ray trajectories inside the cloak are the same as in the ideal cloak (2), however the surface of the cloak may have a nonzero reflectance due to the impedance mismatch [4, 25]. To mitigate the wave reflectance on the surface [4, 25], additional steps can be taken [24, 25]. The advantage of using the reduced parameter set (3) is that only the radial permeability $\mu_r(r)$ varies throughout the cloak, significantly simplifying the design.

The cylindrical cloaks given by (2) and (3) are cylindrically symmetric; that is, they posses continuous rotational symmetry. The underlying coordinate transformation is also cylindrically symmetric, which is only possible if the inner and the outer surfaces of the cloak are both rotationally invariant. Here, we present a general approach to cloaks whose bounding surfaces do not possess such a high symmetry, and, in fact, may not possess any symmetry at all.

First, assume that the inner and the outer boundaries of the cloak are cylinders whose cross-sections can be parameterized in polar coordinates as

$$r = R_{1,2}(\phi), \tag{4}$$

where the indexes 1 and 2 refer to the inner and the outer surfaces, respectively. For example, regular polygons with N sides can be parameterized as follows:

$$r = \frac{r_i}{\cos(\phi \bmod \Phi - \Phi/2)}, \tag{5}$$

where $\Phi = 2\pi/N$ and r_i is the inradius of the polygon, i.e. the radius of the inscribed circle of the polygon. The cloak domain (where the constitutive parameters differ from vacuum) occupies the area described in cylindrical coordinates by $R_1(\phi) < r < R_2(\phi)$. The coordinate transformation that compresses the cross-section of the inner surface to zero can be chosen as follows:

$$r' = \frac{R_2(\phi)}{R_2(\phi) - R_1(\phi)} \left(r - R_1(\phi)\right), \quad \phi' = \phi. \tag{6}$$

This transformation can be rewritten in Cartesian coordinates using $r = \sqrt{x^2 + y^2}$ and $\phi = \arctan(y/x)$. Since the transformation (6) depends on both r and ϕ, the ϵ and μ tensors of the cloak are no longer aligned with the $\hat{r}$ and $\hat{\phi}$ directions of the cylindrical coordinates. Therefore, the expressions for the tensor components are equally involved in cylindrical and Cartesian coordinates. Since our electromagnetic solver requires material

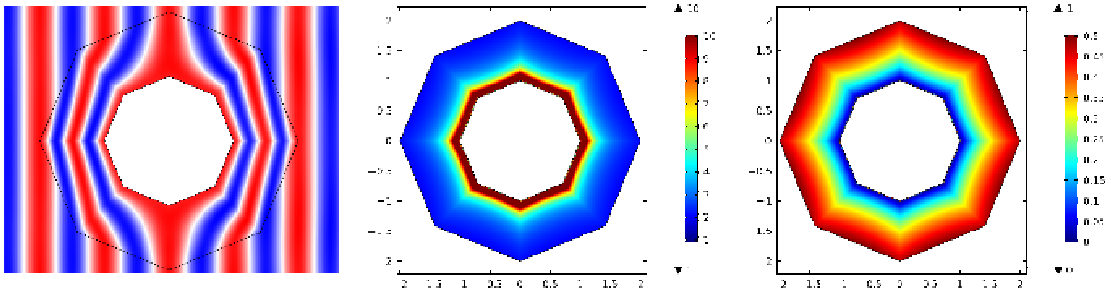

(a) (b) (c)

Figure 2. (Color online) The exact transformation optics octagon-shaped cloak based on the parametrization given by (5,6). (a) Field plot (E_z) for a cloak illuminated by a plane TE wave. (b,c) Distribution of the first (b) and second (c) principal values of the in-plane μ tensor in the cloak.

tensor input in Cartesian coordinates, the formulas below are presented in Cartesian form.

By using $x' = r'\cos(\phi')$ and $y' = r'\sin(\phi')$, we can re-express the transformation (6) in Cartesian coordinates as $x' = x'(x, y)$ and $y' = y'(x, y)$. In terms of the components of the Jacobian matrix of the transformation, defined as $A_{ij} = \partial x'_i/\partial x_j$ with $i, j = 1, 2$ (assuming $x_1 \equiv x$ and $x_2 \equiv y$), the constitutive parameters are then given by [3]:

$$\begin{aligned}
\mu_{xx} &= (A_{xy}^2 + A_{yy}^2)/\det(A), \\
\mu_{xy} &= \mu_{yx} = -(A_{xx}A_{xy} + A_{yx}A_{yy})/\det(A), \\
\mu_{yy} &= (A_{xx}^2 + A_{yx}^2)/\det(A), \\
\epsilon_{zz} &= \det(A),
\end{aligned} \tag{7}$$

where $\det(A) = A_{xx}A_{yy} - A_{xy}A_{yx}$. An example simulation of a cloak whose inner and outer boundaries are shaped as regular octagons is shown in figure 2.

The approach described by (6,7) is applicable to a broad range of shapes, including non-convex shapes, with the only requirement being that the boundaries can be parameterized in cylindrical coordinates in the form (4). For arbitrary shapes, it may be difficult to come up with an explicit analytical parametrization such as the equation given in the polygon example (5). For such general shapes, we have developed a general methodology based on the *wall distance* calculation, a feature available in the COMSOL finite-element solver package [26]. This methodology can be referred to as the *cloaking layer modeling*.

Suppose the surface of the cloak (for concreteness, the inner surface), is drawn within the simulation software, or perhaps, generated from a CAD file. The parametrization of the surface used internally in the software is irrelevant to our technique. In COMSOL, that inner surface can be declared as a *wall*, and the distance D from any point in space to the nearest point on that surface, along with the unit vector N pointing to it, can be found by solving the wall distance equation [26]. The wall distance equation is a variation of the eikonal equation; the equidistant surfaces thus calculated

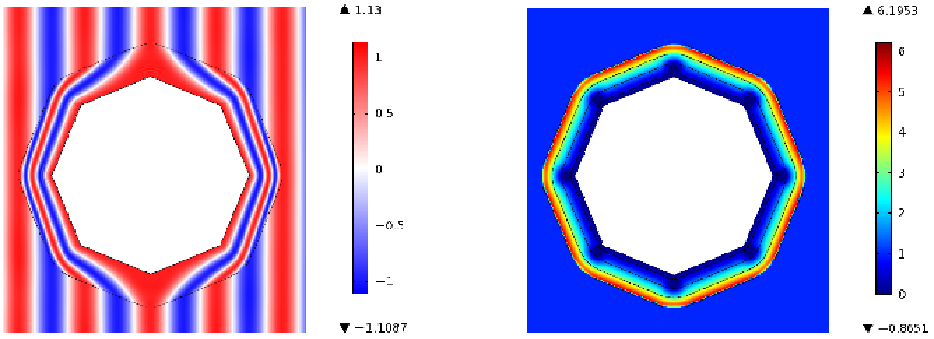

(a) (b)

Figure 3. (Color online) The octagon-shaped cloaking layer based on the parametrization given by (8) and the wall distance equation in COMSOL. (a) Field plot (E_z) for a cloak illuminated by a plane TE wave. (b) Distribution of ϵ_{zz} in the cloak.

can be understood as constant-phase fronts emanating from a fixed-phase boundary. We emphasize that this is merely an approach to parameterizing the cloak inside its volume, and the fact that the eikonal equation is chosen to assist with that has nothing to do with the physical approximations used. Specifically, the structure we are reporting here is an exact, not an eikonal, cloak.

After solving the wall distance equation, the scalar field $D(x, y)$ and the vector field $\vec{N} = -\text{grad}(D)/|\text{grad}(D)|$ are known everywhere, including the volume of the cloaking layer. Using these fields, the cloaking transformation can be written in Cartesian coordinates as follows:

$$x' = \frac{D}{T}\left(x + N_x(T - D)\right),$$
$$y' = \frac{D}{T}\left(y + N_y(T - D)\right), \tag{8}$$

where T is the thickness of the cloaking layer. The inner surface of the cloak corresponds to $D = 0$; in the transformed space its size is reduced to zero. The outer surface of the cloak is an isocontour of the wall distance, $D = T$; this surface remains the same in the transformed space ($x' = x$, $y' = y$). Due to the nature of the wall distance equation, it has to be solved with an additional artificial diffusion term, which, besides improving the solver convergence, provides automatic corner smoothing as a side effect. This side effect can be seen as an advantage, if one has to design a cloaking domain with a non-smooth inner boundary having some corners or edges, and a smooth outer boundary; the wall distance method can provide a continuous transition between such shapes. However, when flat faces joining at a well-defined angle are required both on the inside and outside of the cloak, automatic corner smoothing is an unwanted effect. An example of a cloaking layer grown on the surface of an octagon is shown in figure 3, along with the field distribution of a TE-polarized wave passing through this structure.

Comparing the two TO methods presented in this section, we conclude that the method in which the cloak domain is split into azimuthal sectors and the transformation

is applied to each sector is more suitable for shapes with corners. The piece-wise nature of such transformation preserves the exact shapes of the corners. The second method, based on the wall distance equation, is more appropriate for TO devices with smooth boundaries that do not contain sharp corners or edges.

3. Polygonal approximation of arbitrary-shape cloaks

TO devices can often be realized by collections of metamaterial elements, each designed to provide a local response that approximates the permittivity and permeability tensors at that point. The first step, then, towards implementation of the TO device is the spatial discretization of the otherwise continuous permittivity and permeability distributions. After having accomplished a reasonable discretization, the values of the permittivity and permeability tensors can then be realized by design of the metamaterial elements. While the individual design of the various metamaterial elements would appear straightforward, the spatial arrangement of the elements within the metamaterial represents an impediment to the manufacturability of the TO device.

In the following, we show that the fabrication of TO devices can be significantly simplified if the volume of the TO device is subdivided into flat-faced subsections. In a subsequent refinement to the faceted approximation, the electromagnetic material tensors and the corresponding metamaterial architecture are adequately approximated and simplified within each layer. The proposed method is general and can also be applied to three-dimensional TO objects.

3.1. Description of the approximation methods

Starting from either the exact cloak defined by the constitutive elements of equation (2), or from the eikonal cloak with the reduced constitutive elements of equation (3), we investigate the impact of faceting. Figure 4(a) shows a schematic of the cylindrical cloak, as well as a profile view with the metamaterial elements—here, split ring resonators (SRRs), as were used in the microwave experiments—laid out in a circumferential pattern. The metamaterial elements are the first level approximation to the continuous transformations. If the metamaterial element can control all three of the relevant constitutive tensor elements at a given point, then a discrete approximation to the full transformation is achieved. If the metamaterial element is designed to control only two of the constitutive tensor elements, then the structure represents a discrete approximation to the eikonal cloak.

In this approach, the cylindrical cloak consists of a certain number of concentric rings, each with different radius r. The radius is measured at the radial midpoint of the concentric ring. Each concentric ring is composed of metamaterial elements with identical values of μ_r, μ_ϕ and ϵ_z. The material parameters can be readily obtained from numerical full-wave simulations of a single unit cell in each concentric ring. Although there is no repeated unit cell in the final TO structure, the retrieved effective medium

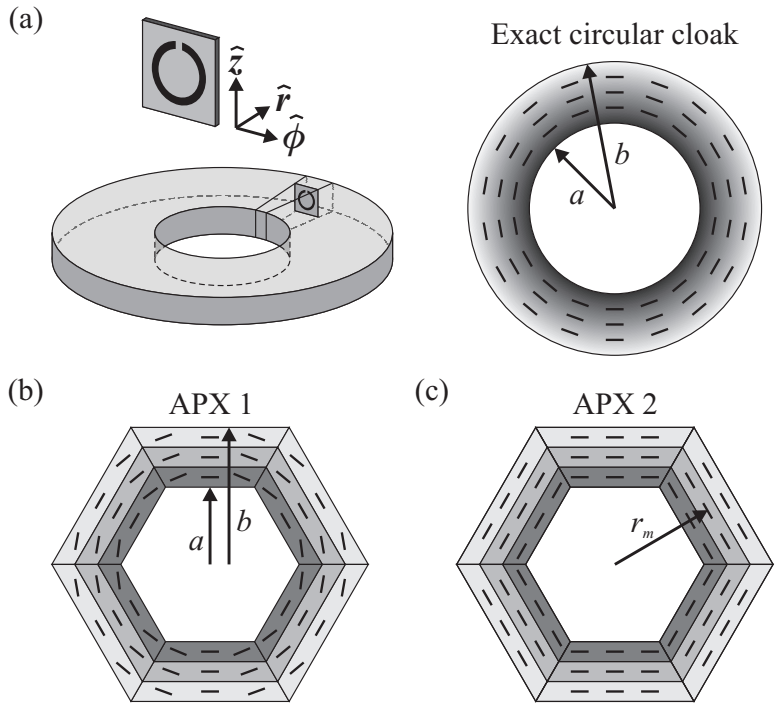

Figure 4. (a) Exact circular cloak consisting of metamaterial elements arranged in concentric circles. (b) and (c) Polygonal cloak shell approximations. In the figures, the grey shading depicts the variation of the geometric dimensions of the metamaterial elements, whereas the short lines indicate the orientation of these elements.

properties for a metamaterial element achieved by assuming periodicity of the element have been shown to be a fairly accurate description, and applicable to gradient and TO media.

Figure 4(b) and 4(c) show two different faceted approximations of the circular cylinder cloak which we refer to as the approximations APX 1 and APX 2, respectively. In both APX 1 and APX 2, the circular cloak is approximated by trapezoid sectors forming a polygon. Consequently, the cloak can be realized by metamaterial elements that are arranged into flat layers that run parallel to the exterior boundary of each sector. By stacking these different layers, the polygonal approximation to a cylindrical cloak is established. The flat metamaterial layers are significantly easier to fabricate using standard lithographic techniques than those with curved boundaries.

We next describe how the ϵ and μ tensors are calculated for the metamaterial elements in each layer in each approximation. For this purpose, we assume that the variation of the cylindrical radius r (which represents the distance from the center) can be neglected within one metamaterial layer.

In APX 1, the continuous tensor fields $\epsilon(r) = \epsilon_z(r)\hat{z}\hat{z}$ and $\mu(r,\phi) = \mu_r(r)\hat{r}\hat{r} + \mu_\phi(r)\hat{\phi}\hat{\phi}$ from the exact circular cylinder cloak are approximated as

$$\begin{aligned} \epsilon_{\text{APX1}}(r) &= \epsilon_z(r_m)\hat{z}\hat{z}, \\ \mu_{\text{APX1}}(r,\phi) &= \mu_r(r_m)\hat{r}\hat{r} + \mu_\phi(r_m)\hat{\phi}\hat{\phi}. \end{aligned} \tag{9}$$

Here, r_m is the radius evaluated at the mid-point of the m-th metamaterial layer in each sector (see figure 4); for example, if the sector spans between angles ϕ_1 and ϕ_2, r_m is evaluated at the mid-angle $\phi_m = (\phi_1 + \phi_2)/2$. In APX 1, the permittivity is thus constant in each layer and each sector, and the permeability tensor has constant principal values but variable principal axes.

In APX 2, we additionally neglect the rotation of the principal axes of the metamaterial elements within each sector. The material tensors are thus given by

$$\begin{aligned} \epsilon_{\mathrm{APX2}}(r) &= \epsilon_z(r_m)\hat{z}\hat{z}, \\ \mu_{\mathrm{APX2}}(r,\phi) &= \mu_r(r_m)\hat{r}_m\hat{r}_m + \mu_\phi(r_m)\hat{\phi}_m\hat{\phi}_m. \end{aligned} \tag{10}$$

Here, $\hat{r}_m$ and $\hat{\phi}_m$ are the unit vectors of the cylindrical coordinate system evaluated at the mid-angle of each sector of the polygon. In APX 2, both ϵ and μ tensors are entirely constant in each layer within each sector; the orientation of the principal axes of μ experiences a jump between sectors (see figure 4(c)).

3.2. Simulation results and discussion

In order to quantify the validity of the different approximations APX 1 and APX 2, we perform numerical calculations and determine the scattering cross-section (SCS) for an exact cylindrical cloak as well as the approximate realizations APX 1 and APX 2. In the model, the mesh size is $\lambda/15$ in regions outside the cloak and 1/5 of the layer thickness (but at most $\lambda/15$) inside the cloak shell. The cloak core is filled with a quasi-perfect electrical conductor with a conductivity of $10^{16}\,\mathrm{S/m}$. To verify the appropriateness of the numerical model, we compute the field distribution for an incident plane wave for the uncloaked core, the exact cloak and for the two approximations APX 1 and APX 2, respectively (see figure 5(a) to (d)). The plots confirm that the two approximations reduce both the backscattering as well as the forward scattering, leading to a field pattern that is qualitatively comparable to that of the exact cloak.

For a quantitative description of the proposed approximations, we calculate the SCS of the different cloaks for an incident plane wave [21]. According to the optical theorem in two dimensions [27], the total cross-section (which includes absorption and scattering) can be determined from the forward scattering amplitude $f(0)$:

$$\sigma_{tot} \equiv \sigma_{sc} + \sigma_{abs} = -2\sqrt{\lambda}\,\mathrm{Re}\{\sqrt{i}f(0)\}, \tag{11}$$

where λ is the wavelength in the medium surrounding the scatterer—in our case, the free space wavelength. The scattering amplitude depends only on the scattering angle and is defined by the asymptotic formula

$$E(r,\phi) \sim E_0\left(e^{ikr} + \frac{f(\phi)}{\sqrt{r}}e^{ikr}\right), \quad r \to \infty, \tag{12}$$

in which r is the distance from the scatterer, E_0 is the amplitude of the incident plane wave, and $k = 2\pi/\lambda$ is the wave number. Thus, in two dimensions $f(\phi)$ has the units of $(\mathrm{length})^{1/2}$, and σ_{tot} has the units of length. For a lossless scatterer, $\sigma_{abs} = 0$ and thus the optical theorem gives the SCS (σ_{sc}) directly without additional calculations. Our

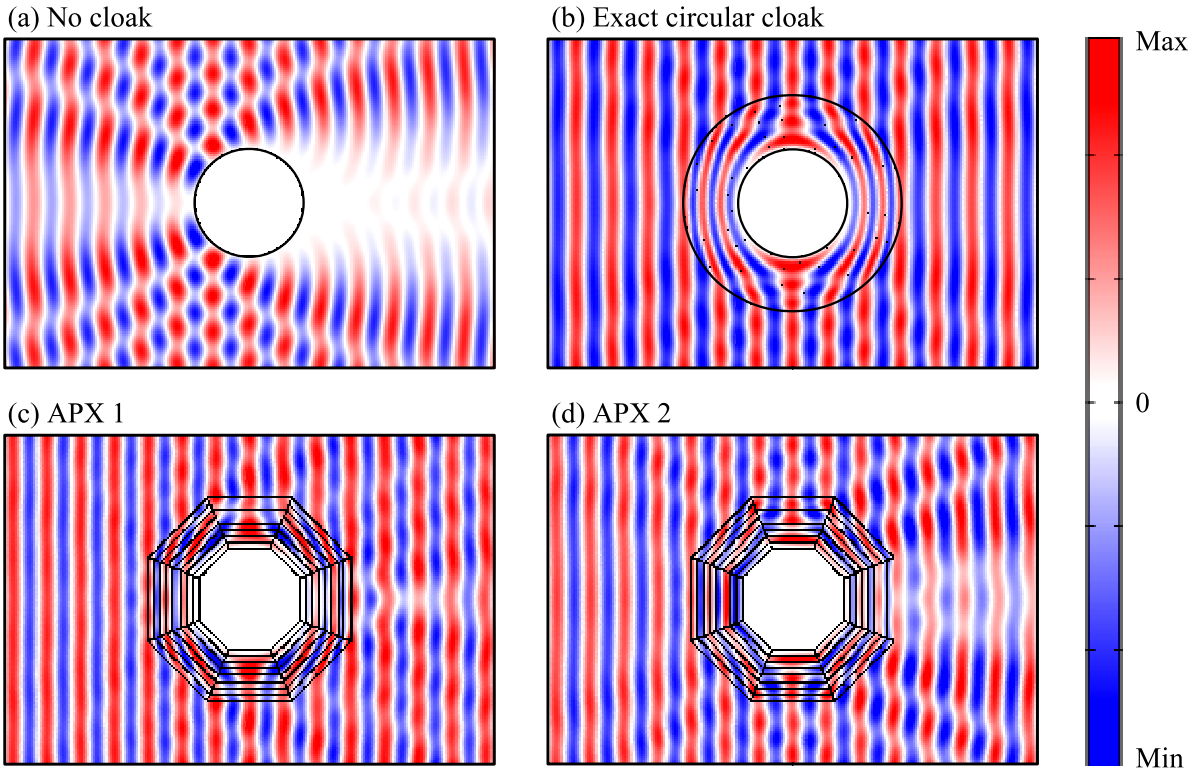

Figure 5. (Color online) Simulation results for the z-component of the electric field of a TE-wave incident from the left. (a) The bare conducting object without a cloak. (b) The exact circular-cylindrical cloak. (c) Approximations APX 1 and (d) APX 2 simulated with the full parameter set.

simulation software permits the calculation of the far-field amplitude in the forward scattering direction; that quantity is linearly proportional to the forward-scattering amplitude in equation (11), which permits us to perform an inexpensive calculation of the total SCS at each frequency.

In the following, we present the SCS for the two approximations APX 1 and APX 2 as a function of the size of the cloaked area, the cloak shell thickness, the number of polygon sides and layers and the angle of wave incidence.

To evaluate the limitations of the proposed models, we first calculate the SCS as a function of the size of the cloak. For this purpose, we vary the radius of the cloaked area from $a = 0.5\lambda$ to $a = 3.5\lambda$ while the outer radius of the cloak is proportionally increased according to $b = 2a$. The corresponding material parameters of the full parameter set (see (2)) are:

$$0 \leq \epsilon_z \leq 2, \quad 0 \leq \mu_r \leq 0.5, \quad 2 \leq \mu_\phi \leq \infty. \tag{13}$$

The diverging behavior of μ_ϕ occurs only near the inner boundary of the cloak where the electromagnetic fields are negligibly small. Therefore, in an explicit metamaterial implementation, the limited nature of the effective permeability produces only a small error in this region. For the reduced parameter set of (3), however, all material

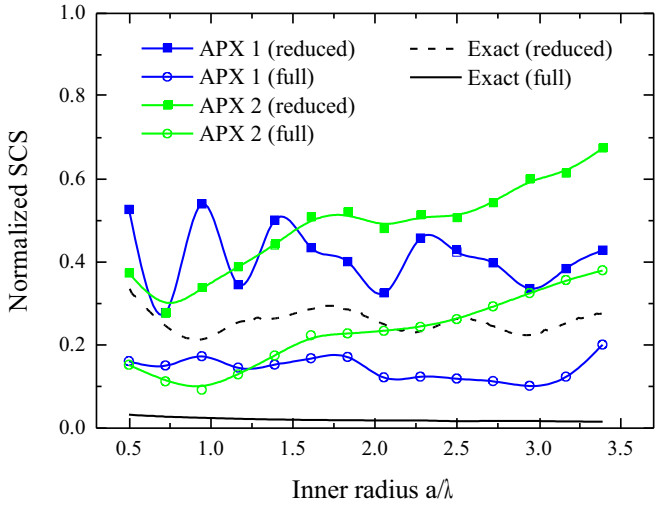

Figure 6. (Color online) Scattering cross section (SCS) normalized to the SCS of the bare conducting core for the proposed approximations APX 1 and APX 2 in dependence on the core radius a for a constant cloak shell ratio $b = 2a$ and a 10-sided polygon. The black lines show the corresponding SCS of the exact circular-cylindrical cloak.

parameters remain finite:

$$\epsilon_z = 4, \quad 0 \leq \mu_r \leq 0.25, \quad \mu_\phi = 1. \tag{14}$$

Note that the parameter ranges of both the full and the reduced parameter set are independent of the size of the cloaked area which means that all cloak sizes can be realized by the same set of metamaterial elements.

In figure 6, we show the resulting SCS, normalized to the SCS of the bare conducting core for the two approximations and for both the full and the reduced parameter set. To achieve sufficient cloaking even for a large cloak, we assumed a 10-sided polygon for all models. Furthermore, the number of layers in each polygon section was step-wise increased with increasing size of the cloak (starting with 5 layers) to keep the layer thickness smaller than $\lambda/10$. For comparison, we have also plotted in figure 6, the SCS of the exact circular-cylindrical cloak for the full and the reduced parameter set, respectively (solid and dashed black lines).

As expected, the models that are based on the full parameter range (indicated by small circles) generally provide a better cloaking ability than the models with reduced parameter set (small squares) with a reduction of the SCS of about a factor of two. For the considered cloak core sizes, the SCS of model APX 1 is nearly independent of the size and reaches values around SCS = 0.15 if the model is initialized with the full parameter set (blue line with circles) and SCS = 0.41 for a cloak based on the reduced set (blue line with squares). In contrast to this stable behavior, the SCS of the model APX 2 slightly increases with increasing core size and approaches values of about 0.45 for the full parameter set and 0.70 for the reduced set as the core size approaches an inner radius of $a = 3.5\lambda$. The increasing SCS for the model APX 2 is a direct consequence of the

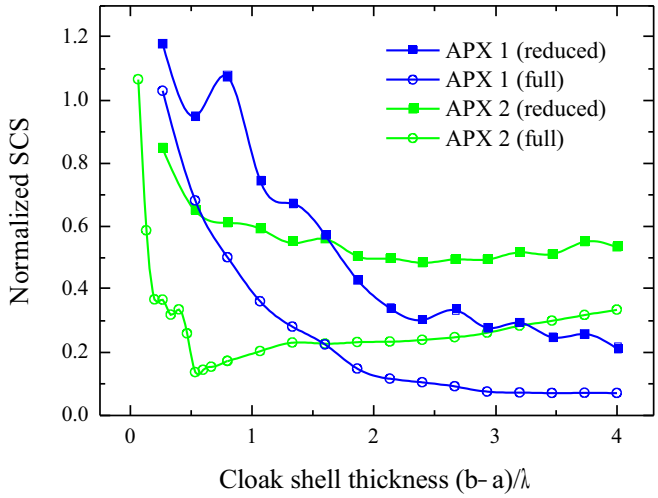

Figure 7. (Color online) Scattering cross section (SCS) normalized to the SCS of the bare conducting core for the proposed approximations APX 1 and APX 2 in dependence on the cloak shell thickness for a constant core radius $a = 2\lambda$ and a 10-sided polygon.

stronger approximations made in this model (as shown later, this can be compensated by increasing the number of polygon edges).

Once the area to be cloaked is specified, the cloak can still be optimized by varying the size of the cloak shell. Therefore, we determined the cloaking performance of the different approximations with respect to the thickness of the cloak shell $(b - a)$ for a constant inner radius of $a = 2\lambda$ and for a 10-sided polygon. As before, the number of layers in each polygon section was stepwise increased with growing outer radius b such that the thickness of each layer was $\lambda/10$ at most. The resulting SCS for the two approximations in dependence on the normalized shell thickness $(b - a)/\lambda$ is plotted in figure 7.

The total dependence of the SCS on the cloak shell thickness is a combination of several effects. First, if the cloak shell is very thin, the distribution of the material parameters is compressed into a small region of space. This leads to a large jump of the material parameters at the interface between adjacent layers (in which the parameters are constant) and thus to an increased scattering of light. Consequently, the SCS for all models gets very large as the cloak shell thickness tends to zero. Second, for the models that are based on the reduced parameter set, the wave impedance of the outer cloak boundary $z = \sqrt{\mu_\varphi/\epsilon_z} = 1 - a/b$ (see (3)) approaches that of free space as the outer boundary b increases (a is fixed). This leads to a decreasing scattering. On the other hand, if the shell thickness increases, the role of spatial imperfections, i.e. the deviations from the exact material parameters at a given point, gain significance and lead to an enhanced scattering. This is especially the case for the model APX 2 which includes stronger approximations than model APX 1.

For the considered realizations, the net effect for the model APX 1 is a general decrease of the SCS for increasing shell thicknesses (see blue lines in figure 7).

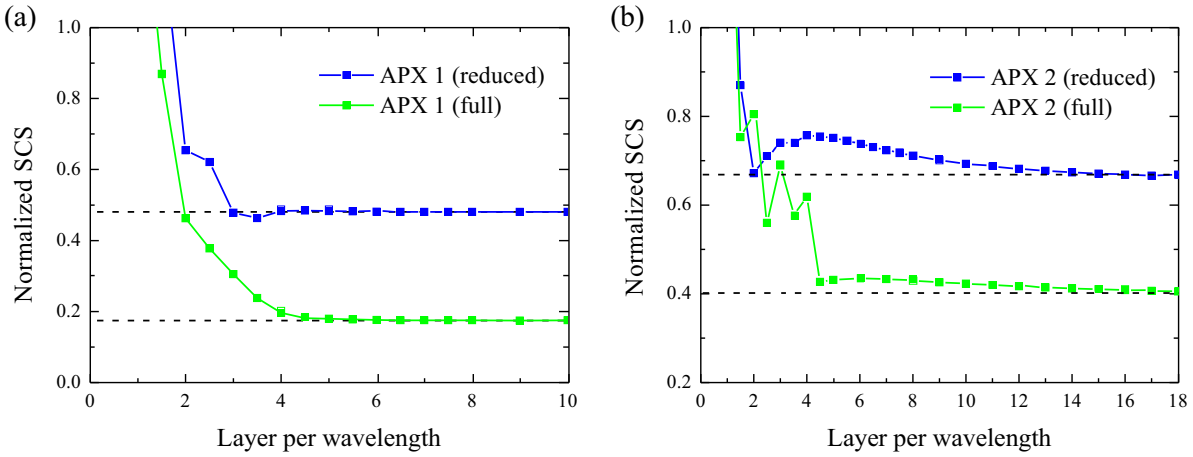

Figure 8. (Color online) Normalized scattering cross section (SCS) in dependence on the package density of the metamaterial layers simulated with the full parameter set (red dotted line) and the reduced (black dotted line) parameter set.

Obviously, within the considered thickness range, the improved impedance matching for larger cloaks exceeds the adverse effect of the increasing spatial imperfections. The corresponding SCS approaches a minimal value of 0.21 for the reduced parameter set and 0.07 for the full parameter set, respectively. In contrast, for the model APX 2 the impact of spatial imperfections becomes more crucial. For the full parameter set (green line with small circles in figure 7), the imperfections start to overcompensate the improved impedance matching at a shell thickness of 0.5λ leading to a local scattering minimum where the SCS decreases to 0.14. Yet, the corresponding curves of the reduced parameter set show a more stable behaviour with an almost thickness-independent SCS around 0.6 (see green line with small squares in figure 7). Here, the two counter effects of the increasing imperfections and the improving impedance matching are almost balanced.

In order to estimate the fabrication effort of the layered cloaks, we next investigate the number of layers that are necessary to provide a reasonable cloaking effect. In figure 8(a) and (b) we show the normalized SCS as a function of the number of layers for model APX 1 and APX 2 for both the reduced and the full parameter set, respectively. The assumed geometry of the cloak was an 8-sided polygon with an inner radius of $a = 2\lambda$ and an outer radius of $b = 4\lambda$.

The curves show a fast convergence towards a constant SCS which corresponds to a quasi-continuous distribution of the material parameters within the cloak. Obviously, a sufficient convergence is already achieved for a package density of 4 layers per wavelength for model APX 1 (figure 8(a)) and for 6 layers per wavelength for model APX 2 (figure 8(b)). Below this limit, the major contribution to the SCS arises from internal reflections between adjacent layers. In this regard, the full and the reduced parameter set lead to a similar SCS of the cloak. In other words, the higher effort of using metamaterial elements that provide a full parameter set is only reasonable if the thickness of the layers is smaller than $\lambda/4$ for model APX 1 and smaller than $\lambda/8$ for model APX 2, respectively.

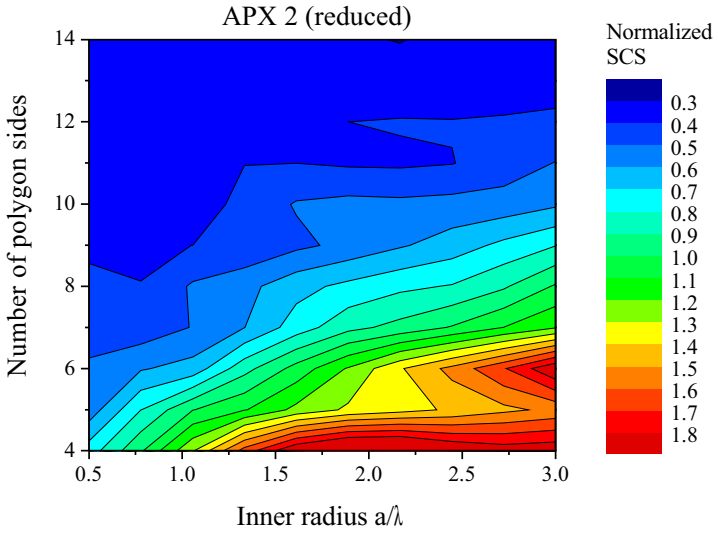

Figure 9. (Color online) Normalized scattering cross section (SCS) in dependence on the inner radius a of the cloak and the number of polygon sides for the approximation APX 2. The simulations are based on the reduced parameter set and refer to a cloak with an outer radius of $b = 2a$.

But this weak condition is usually satisfied in common metamaterial implementations.

Next, we determine the number of necessary polygon sides in dependence on the area to be cloaked. For short, we exemplarily show this dependence only for the reduced parameter set of model APX 2 since this is the most interesting configuration for a practical realization. As before, the outer radius b was proportionally increased with increasing inner radius a according to $b = 2a$ to ensure that the same material parameter range is covered as in the preceding discussion, and we assumed a layer thickness of about $\lambda/10$.

The resulting normalized SCS in dependence on the inner radius a and the number of polygon sides N is shown as a 2D plot in figure 9. As expected, the number of necessary polygon sides increases for an increasing cloak size. For example, if we intend to reduce the SCS of the cloak below 50 % of the SCS of the uncloaked core, the minimum number of polygon sides is $N = 7$ for an inner radius of $a = 0.5\lambda$ and $N = 11$ for $a = 3\lambda$. For more than 12 polygon sides, there is no significant further reduction for all analyzed sizes.

As a final aspect of the proposed polygonal approximations, we analyze the influence of the orientation of the cloak with respect to the incident wave. Since the polygonal shape breaks the rotational symmetry of the original cylindrical cloak, the used approximations are expected to be sensitive to the angle of incidence. This angle dependence is exemplarily shown in figure 10 where we have plotted the normalized SCS of the models APX 1 and APX 2 as a function of the angle of incidence. The calculations are based on the full parameter set and we considered an 8-sided polygon (figure 10(b)), as well a 9-sided polygon (figure 10(a)). In the simulations, we assumed

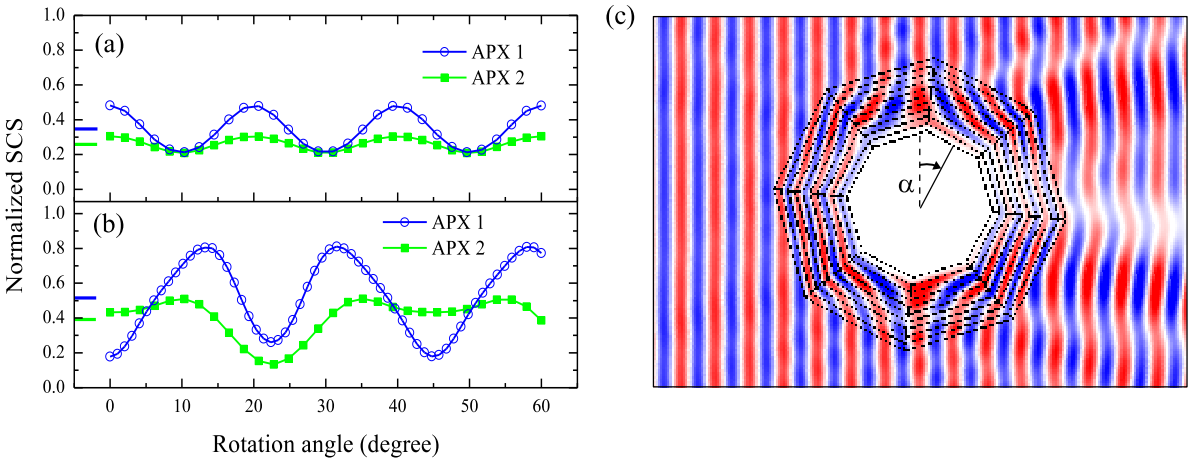

Figure 10. (Color online) (a) Normalized scattering cross section (SCS) in dependence on the angle of incidence for a 9-sided polygonal cloak calculated for the full parameter set. The angle of 0° corresponds to the case where the wave incidence is normally to a polygon side. (b) Same as (a), but for an 8-sided polygon. The short lines at the y-axis indicate the annularly averaged SCS. (c) z-component of the scattered electric field, exemplarily shown for an incident angle of 17° for the 8-sided version of APX 2.

an inner and outer radius of $a = 2\lambda$ and $b = 4\lambda$, respectively, and 10 layers in each polygon section.

The resulting curves plotted in figure 10(b) show a periodic modulation which mirrors the expected 45° annular period of the 8-sided polygon. In contrast, the curves calculated for the 9-sided polygon (see figure 10(a)) display a period of only 20° i.e. only the half of the expected 40° period of an 9-sided polygon. The reason for the higher symmetry is the odd number of polygon sides as can be explained as follows: there are two symmetric orientations of a polygonal cloak with respect to the incident wave. The first occurs if a polygon side is normal to the incident wave (case 1) and the second occurs if a vertex of the polygon points towards the source (case 2). If the polygon has an even number of sides the two cases possess different SCS because the front and the back of the cloak are either two parallel sides (case 1) or two opposing vertices (case 2). However, if the number of polygon sides is odd, a side is always opposite to a vertex and thus the two cases have a comparable geometry. This leads to similar values of the SCS and thus to a halving of the annular period.

Furthermore, the curves in figure 10 show that model APX 2 generally provides a more stable SCS under cloak rotation than model APX 1, and also the annularly averaged SCS of APX 2 is smaller than that of APX 1. For example, for an 8-sides polygon (see figure 10(b)) the mean value and standard deviation of the averaged SCS are 0.51 ± 0.21 for model APX 1 but only 0.39 ± 0.12 for model APX 2.

In summary, both polygonal approximations of the exact cylindric cloak show a comparable and reasonable cloaking performance. For a given size of the area to be cloaked, the reduction of the SCS can be optimized by varying the size of the cloak

shell and the number of polygon edges. For the analyzed sizes ($a \leq 3.5\lambda$) and realistic geometric dimensions, we achieved a reduction of the SCS on the order of 10 % of the uncloaked core. In general, model APX 1 provides a slightly better cloaking figure-of-merit, since the SCS shows a faster decrease with increasing cloak thickness; on the other hand, APX 2 is less sensitive to the angle of incidence. For both models, the role of inter-layer reflections is negligible as long as the layers of metamaterial elements are thinner than $\lambda/4$ (APX 1) or $\lambda/8$ (APX 2), respectively, which is also a realistic assumption for a practical implementation. From the ease-of-fabrication point of view, model APX 2 has the advantage that the metamaterial elements are all identically aligned within one layer. Such uniform, flat layers can be manufactured even with the micro- and nanoscale dimensions by standard fabrication methods.

4. Conclusion

In this paper, we have proposed an approximation method for the design of transformation-optical (TO) components of arbitrary shape. Starting from the exact transformation, a polygonal approximation of the curved shape of the TO device is introduced. In consecutive approximations the metamaterial elements were aligned parallel to the flat boundaries of the polygons. As a major advantage, the polygonal approximation significantly mitigates the fabrication constraints since the resulting TO components can be implemented by flat metamaterial layers. This can be readily achieved by standard lithographic and stacking techniques. We have validated the approach for the example of a cylindrical cloak and quantified the accuracy of the approximations by comparing the scattering cross-section of the cloak with the exact TO cloak of a circular shape.

Furthermore, we have presented an alternative method for the design of electromagnetic cloaks with virtually arbitrary shapes. The approach is based on the *wall distance* calculation and is applicable to a large class of cloak geometries including convex shapes and even some non-convex shapes. The new technique has been numerically verified on a specific example of an octagon-shaped cloak.

Acknowledgments

This work was partially supported through a Multidisciplinary University Research Initiative, sponsored by the U.S. Army Research Office (Contract No. W911NF-09-1-0539). The authors are thankful to Christian Wollblad (COMSOL AB) for assistance with the wall distance equation.

References

[1] Pendry J B, Schurig D and Smith D R 2006 *Science* **312** 1780–1782
[2] Rahm M, Cummer S A, Schurig D, Pendry J B and Smith D R 2008 *Phys. Rev. Lett.* **100** 063903
[3] Kundtz N B, Smith D R and Pendry J B 2010 *Proc. IEEE* **PP:99** 1–12 ISSN 0018-9219

[4] Schurig D, Mock J J, Justice B J, Cummer S A, Pendry J B, Starr A F and Smith D R 2006 *Science* **312** 977–980
[5] Cai W, Chettiar U K, Kildishev A V and Shalaev V M 2007 *Nature Photon.* **1** 224 – 227
[6] Landy N I, Kundtz N and Smith D R 2010 *Phys. Rev. Lett.* **105** 193902
[7] Leonhardt U 2011 *Nature* **471** 292293
[8] Novitsky A, Qiu C W and Zouhdi S 2009 *New Journal of Physics* **11** 113001 URL http://stacks.iop.org/1367-2630/11/i=11/a=113001
[9] Qiu C W, Hu L, Xu X and Feng Y 2009 *Phys. Rev. E* **79** 047602
[10] Ruan Z, Yan M, Neff C W and Qiu M 2007 *Phys. Rev. Lett.* **99** 113903
[11] Kwon D H and Werner D H 2008 *Applied Physics Letters* **92** 013505 (pages 3) URL http://link.aip.org/link/?APL/92/013505/1
[12] Rahm M, Schurig D, Roberts D A, Cummer S A, Smith D R and Pendry J B 2008 *Photonics and Nanostructures-fundamentals and Applications* **6** 87–95
[13] Popa B I and Cummer S A 2010 *Phys. Rev. A* **82** 033837
[14] Han T, Qiu C and Tang X 2010 *Journal of Optics* **12** 095103 URL http://stacks.iop.org/2040-8986/12/i=9/a=095103
[15] Nicolet A, Zolla F and Guenneau S 2008 *Opt. Lett.* **33** 1584–1586 URL http://ol.osa.org/abstract.cfm?URI=ol-33-14-1584
[16] Li C and Li F 2008 *Opt. Express* **16** 13414–13420 URL http://www.opticsexpress.org/abstract.cfm?URI=oe-16-17-13414
[17] Jiang W X, Chin J Y, Li Z, Cheng Q, Liu R and Cui T J 2008 *Phys. Rev. E* **77** 066607
[18] Wang X, Qu S, Xia S, Wang B, Xu Z, Ma H, Wang J, Gu C, Wu X, Lu L and Zhou H 2010 *Photonics and Nanostructures - Fundamentals and Applications* **8** 205–208
[19] Soukoulis C M and Wegener M 2011 *Nature Photonics* 10.1038/nphoton.2011.154
[20] Urzhumov Y A and Smith D R 2010 *Phys. Rev. Lett.* **105** 163901
[21] Urzhumov Y A, Kundtz N B, Smith D R and Pendry J B 2011 *Journal of Optics* **13** 024002 URL http://stacks.iop.org/2040-8986/13/i=2/a=024002
[22] Tao H, Strikwerda A C, Fan K, Bingham C M, Padilla W J, Zhang X and Averitt R D 2008 *J. Phys. D: Appl. Phys.* **41** 232004
[23] Kundtz N B, Gaultney D and Smith D R 2010 *New J. Phys.* **12** 043039
[24] Urzhumov Y, Ghezzo F, Hunt J and Smith D R 2010 *New Journal of Physics* **12** 073014 URL http://stacks.iop.org/1367-2630/12/i=7/a=073014
[25] Cai W, Chettiar U K, Kildishev A V, Shalaev V M and Milton G W 2007b *Applied Physics Letters* **91** 111105 (pages 3) URL http://link.aip.org/link/?APL/91/111105/1
[26] COMSOL AB Stockholm, Sweden 2010 *COMSOL Multiphysics User's Guide, Version 4.1*
[27] Boya L J and Murray R 1994 *Phys. Rev. A* **50** 4397